

Evaluating the Extraction Approaches of Flood Extended Area by Using ALOS-2/PALSAR-2 Images as a Rapid Response to Flood Disaster

A. Besse Rimba, Fusanori Miura

Department of Environmental Science and Engineering, Yamaguchi University, Tokiwadai, Ube City, Japan

Email: a.besserimba@yahoo.com

How to cite this paper: Rimba, A.B. and Miura, F. (2017) Evaluating the Extraction Approaches of Flood Extended Area by Using ALOS-2/PALSAR-2 Images as a Rapid Response to Flood Disaster. *Journal of Geoscience and Environment Protection*, 5, 40-61.

<http://dx.doi.org/10.4236/gep.2017.51003>

Received: December 25, 2016

Accepted: January 13, 2017

Published: January 16, 2017

Copyright © 2017 by authors and Scientific Research Publishing Inc. This work is licensed under the Creative Commons Attribution International License (CC BY 4.0).

<http://creativecommons.org/licenses/by/4.0/>



Open Access

Abstract

Flash floods are recurrent events around the Japan region almost every year. Torrential rain occurred around Kanto and Tohoku area due to typhoon No. 18 in September 2015. Overflowing of the Kinugawa River led to river bank collapse. Thus, the flood extended into Joso City, Ibaraki Prefecture, Japan. ALOS-2/PALSAR-2 was the fastest satellite to record this flood disaster area. A quick method to extract the flood inundation area by utilizing the ALOS-2/PALSAR-2 image as a rapid response to the flood disaster is required. This study evaluated three methods to extract the flood immediately after the flood occurring. This study compared the extraction approaches of flooded area by unsupervised classification, supervised classification and binary/threshold of backscattering value of flood. The results show that unsupervised classification and supervised classification are overestimated. This study recommends the binarization of the backscattering value to extract the extended flood area. This method is a straight forward approach and generates a similar distribution with the field survey by using the aerial photo with high accuracy (94% of kappa coefficient). We utilized slope map which derived from DEM data to eliminate the overestimated area due to shadowing effect in SAR images.

Keywords

Flood, ALOS-2/PALSAR-2, Rapid Response, Unsupervised and Supervised Classification, Binarization

1. Introduction

In recent years, natural disasters have frequently occurred in many parts of the world. Early detection of the damage situation is important. It is possible to recognize early damage status by using the satellite of remote sensing technology because it can show disaster phenomena. Remote sensing technology can be uti-

lized in the various phases of disaster management, e.g., prevention, preparedness, relief and reconstruction [1]. From 2004 to 2015, 90% of disasters had been related to the weather and 47% of those were associated with flooding [2].

Remote sensing is a helpful tool to detect change because of the satellite repeatedly visiting the same area after short intervals of time and with consistent spatial resolution while utilizing the same sensor [3]. Some studies have been done using remote sensing to detect the land change [4] [5] [6] [7]. The application of remote sensing in disaster management is widespread [8] [9] [10].

Flash flood is defined as a quick onset of a flood with a short-term duration and a moderately high peak outflow [11]. It happens quickly, commonly within six hours of rainfall, and is sometimes followed by debris flows, mudflows, bridge and river bank collapse, and damage to infrastructures and houses [12]. The height of flash floods can exceed 10 m (~30 ft) [13]. Remote sensing has been applied to flash flood studies, including flash flood monitoring by the near-infrared Lidar [14], flash flood prediction by remotely-sensed precipitation [15], and flash flood damage mapping [16].

Some studies have been done by previous researchers to detect flash floods. Kuldeep and Garg investigated floods by using image fusion of Cartosat-1 and Resourcesat-1 [17]. By using object-based classification, they categorized the land cover into nine classes with segmentation scale 80. They utilized the panchromatic image to extract the flood. It can be possible to utilize the panchromatic data once the rain has finished and the water has inundated for a few days. Hence, the panchromatic image is powerless to apply to extracting the flood immediately during torrential rains [18]. During a flood event, radar sensors are the best sensors to detect the inundation area; radar measures the returned signal, *i.e.* backscatter, and can measure the terrain regardless of the weather and time [19] [20] [21] [22]. Water has low backscattering in SAR images [23] because water has a smooth surface [24]. The water area is shown as a dark area in SAR images because the signal directly reflects like a mirror reflection on smooth surfaces. Manjstree *et al.* investigated the best polarization to extract the flood by using RADARSAT-2. They concluded that transmitted horizontal and received horizontal (HH) polarization was better than transmitted horizontal and received vertical (HV) polarization, transmitted vertical and received horizontal (VH) polarization, and transmitted vertical and received vertical (VV) polarization [25]. Pierdicca *et al.* investigated the flood inundation area by integrating ERS-1 imagery, land cover map and DEM data [26]. Mason *et al.* detected flooding in an urban area by applying TerraSAR-X and Lidar data to eliminated effects of shadow and layover [27].

Typhoon 18 passed through Japan and caused torrential rain from West Japan to Northern Japan. The typhoon brought heavy rainfall to Tohoku and Kanto area. From September 7 to 11, the rainfall intensity exceeded 500 mm for the Tohoku region and 600 mm for the Kanto region. Especially in Tochigi Prefecture, the rainfall intensity was observed by 16 observation points that reached 550 mm during the 24 hours from September 10 to 11, 2015. In Aichi Prefecture,

the typhoon passed through from 9:30 am on September 9th, 2015 and proceeded to the Japan Sea at 3 pm that caused the low pressure. As a result, the heavy rain occurred during the evening [28] [29] and caused the river bank collapse in the middle of the night. Heavy rainfall occurred from 9th to 11th September engendering the flood in Joso City, Ibaraki, Japan. The Japanese government's Fire and Disaster Management Agency and other national and local governments reported 12,088 flooded homes [28] [29].

ALOS-2 PALSAR-2 as the first satellite to record the flooded area in Joso City has a major role in a rapid flood response. This satellite was designated to visit the disaster-prone area around Sentinal Asia member (Asia Pacific) immediately after the disaster occurring. It has high spatial resolution; one pixel represents 1 m to 3 m [30]. Thus, it should be suitable for flood inundation areas detection in urban and rural area [31] [32]. In addition, PALSAR-2 also provides a number of data observation angles which can enhance the number of prospects and accuracy for flood observations [33]. ALOS-2 PALSAR-2 image also has been utilized for monitoring and extraction flooded areas [33] [34] [35]. In the case of the flood in Joso City, the ALOS-2/PALSAR-2 recorded the flood area at 2:43 am, a few hours after the flood occurred. This means that rapid data from this satellite is available when a disaster occurs. A rapid disaster prone extraction method is required to identify needs, deliver supplies and save lives. The aim of this study was to evaluate the extraction methods of the flooded area by a quick method using satellite images, because rapid flood inundation extraction and delivery of flood inundation maps during a flood period can support crucial information for government and decision makers to highlight relief and rescue processes.

Hence, this study compared methods to extract the flood data for a rapid response to the flash flood. The extraction of flood data used three methods; unsupervised classification [36], supervised classification [35] and binarization or thresholding of backscattering value [37]. Some researchers investigated these methods to flood. Vassileva *et al.* investigated flooding in Ljubljana (Slovenia) by extracting the shadow using unsupervised classification and utilizing RADARSAT-2 images combining with Shuttle Radar Topography Mission (SRTM) images with 90m of spatial resolution [36]. The advantage of this research was an application in a wide area without training area. Yamasaki and Liu had analyzed Joso City by using ALOS-2/PALSAR-2 that recorded September 10th, 11th, 13th and October 10th 2015 by classifying the land cover [35]. They also extracted the water body by using 5m DEM data. According to their study, the peak of the flood was on 11th September 2016. As known, the flood in Joso City occurred due to the bank collapse. Their result was unable to show the bank collapse by using their flood extraction method. Yamasaki and Liu applied some data to monitoring the distribution of the flood inundation. Hong *et al.* studied the water area extraction by thresholding and integrating the RADARSAT SAR imagery, Landsat imagery and DEM data [37]. They utilized Landsat 5 TM to extract the land use by unsupervised classification, extract water from RADA-

RSAT SAR imagery by thresholding the backscattering of water and topography correction by applying DEM data. All the studies offered method using SAR images (medium and high-resolution data) for detecting the flood. However, no study has compared the effective method and high accuracy using ALOS-2/PALSAR-2 (high-resolution data) for flood detection.

This study intended to extract the flash flood as a rapid response. This study evaluated three methods to extract the flooded area in Joso City during the flood on 10th September 2015. Two of the approaches used are land cover classification and one method uses binarization or threshold of backscattering value. A straightforward and informative method was required to fulfill flash flood extraction as a rapid response. The method should trim the long processing time. All the methods were verified by using the aerial photo as a field survey. ALOS-2 PALSAR-2 as SAR image has a disturbance, e.g., speckle and shadowing that caused the overestimating the inundated area. The speckle noise was removed by applying double filter [38] and shadowed area was removed by slope map [27].

2. Study Area and Dataset

2.1. Study Area and Flood Experience

Joso City is positioned in the southwestern part of Ibaraki prefecture and approximately 55 km from Tokyo. Its width is approximately 20 km north-south and 10 km east-west with a total area of 123.52 km². The relief of the city has flat land with some low hills with altitude 5 - 24 meters above sea level. Joso City has four seasons as a typical example of the Pacific Ocean temperate zone [39].

Kinugawa River passes almost through the central part of Joso City running from north to south. The east side of the river has become a broad area of rice because of the lowland. The west region of the river has low hills and spread farms, villages, cultivated fields, widespread woods-plains; and is being developed with the development of industrial places, residential plazas, golf courses, and so on, as one of the strategic areas of Tokyo Metropolitan Region, strengthening urban structure roles. According to the Statistics data as of 1st January 2015, Joso City has population 65,370 people [39]. **Figure 1** displays the study area.

Before the flood control (*i.e.*, dam) was established in the upstream of Kinugawa River, flood used to occur due to the heavy rain (e.g., September 1935, September 1938, September 1947, August 1949, September 1982 and July 2002) [40]. However, the heavy rainfall occurred in September 2015 and caused flash flood in east part of Joso City due to the river bank collapsed. Flood inundated for a few days in Joso City [29] and caused two people die, more than 40 injured people and more than 5000 extremely destroyed houses [39]. The number loss of life and material lead the rapid response to the flood. Thus, this study was applied in Joso City as the study case for rapid response to the flood.

2.2. Dataset

This study utilized three kinds of data. Digital Elevation Model (DEM), 5 meter

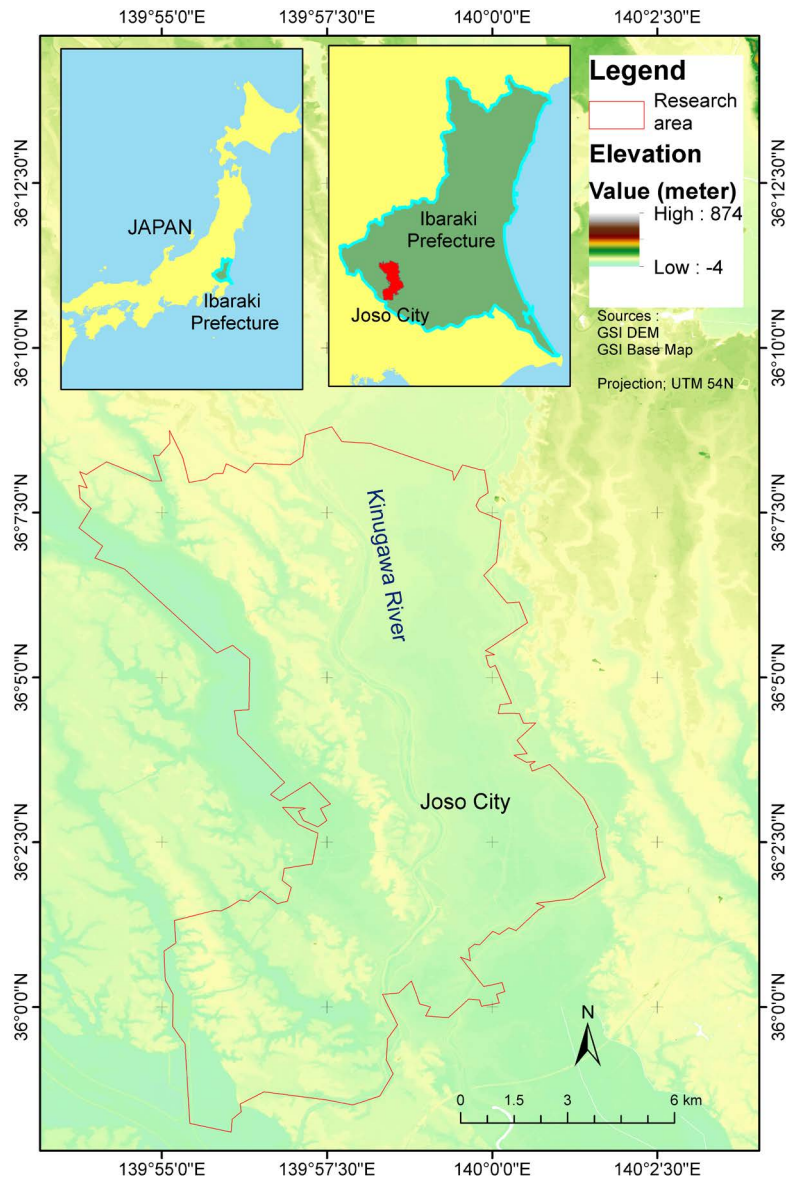


Figure 1. Study area (source; GSI DEM).

accuracy, was provided by The Geospatial Information Authority of Japan (GSI) with Geography Markup Language (GML) format. We utilized this data to generate the slope map; Aerial photo (recorded September 9th, 2015) during flooding in Joso City; it was provided from GSI in order to verify the extraction methods. ALOS-2/PALSAR-2 images provided by the Japan Aerospace Exploration Agency (JAXA) as listed in **Table 1**.

3. Methodology

3.1. Overview

In this study, unsupervised classification and supervised classification classified the land use and detected the land use change. Binarization method extracted the backscattering of water. We used only SAR images (pre- and post-disaster)

Table 1. Specification ALOS-2/PALSAR-2 images for this study.

Satellite	Date	Image	Observation direction	Off-nadir	Polarization	Resolution
PALSAR-2	2015/9/10	Post-disaster	Descending	35.8°	HH	3 m
	2015/7/31	Pre-disaster	Descending	35.8°	HH	3 m

to extract the land cover and flood inundation. Field survey verified the extraction flood; the distribution which has similar distribution with the field survey was selected as the recommended method. Overestimation of the flood area by using SAR image could be reduced by superimposing to slope data. We decided the margin of slope data according to the flood distribution of field survey. Otherwise, the limitation of SAR image in settlement area (e.g., double bounce) was not included in this study. The flowchart of proposed methods is displayed in **Figure 2**.

Three methods were applied to extract the flood inundation in Joso City when the flood was occurring in September 2015 by utilizing the ALOS-2/PALSAR-2 images. All these methods utilized pre- and post-flood of SAR images. Post-disaster image refers to an image recorded during the flood. We applied unsupervised classification as the first method and supervised classification as the second method to classify the land use pre- and post-disaster. Land use classification of pre- and post-disaster image were superimposed to find the land use change. The third method was extracting the water backscattering from pre- and post-disaster and deciding the threshold of the flood inundation, *i.e.*, binary/backscattering threshold method. The change area from pre- and post-disaster image is identified as the inundation of flood.

3.2. Backscattering

The first step of processing the ALOS-2/PALSAR-2 data was converting from the digital number (DN) to the backscattering coefficient (sigma-naught) in order to generate the value of backscattering of the object. It denotes as dB and can be found by the following Equation (1) [30].

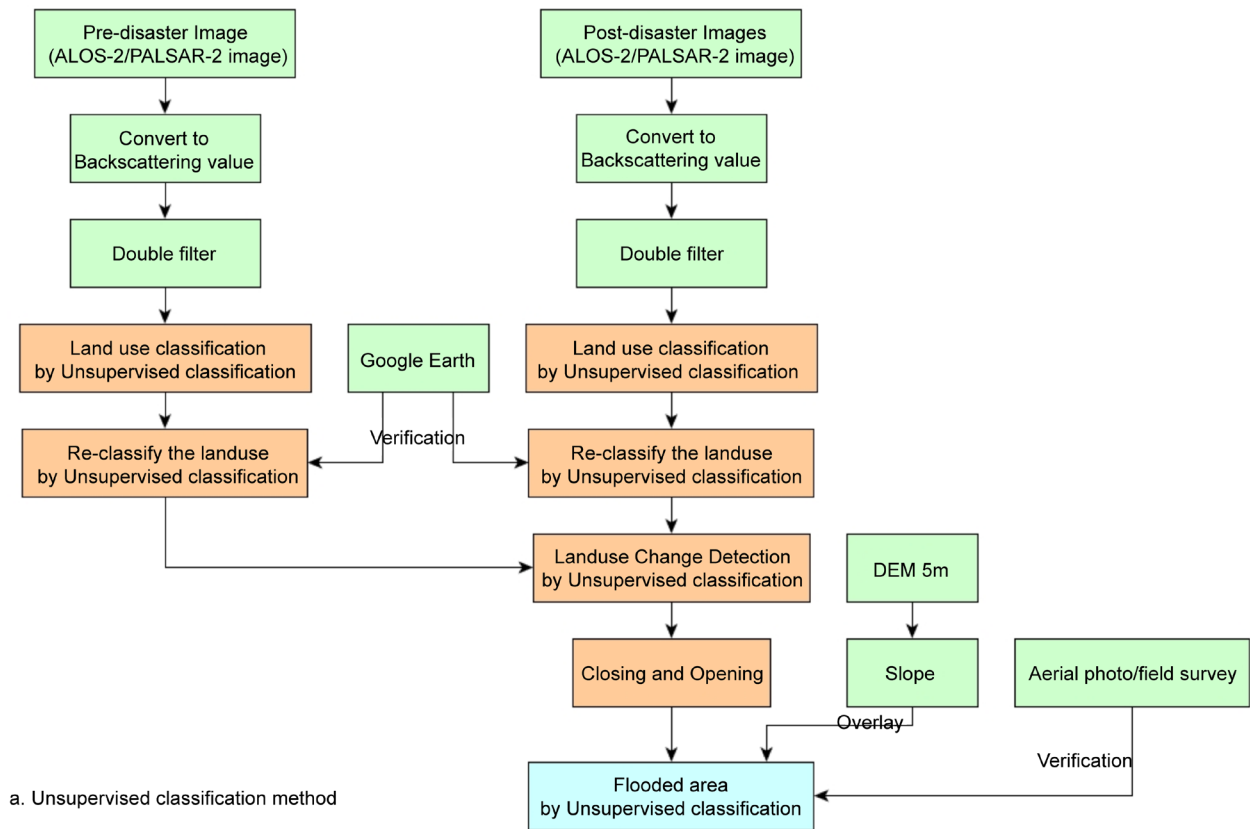
$$\sigma^o = 10 \log_{10} (\text{DN}^2) + \text{CF} \quad (1)$$

where: σ^o is backscattering coefficient; DN is a digital number; Calibration Factor (CF) for ALOS-2/PALSAR-2 are -83 as listed in **Table 2** [41]. CF can be calculated by following Equation (2); where A_x is area of the compound and C_x is concentration of the compound.

$$\text{CF} = A_x / C_x \quad (2)$$

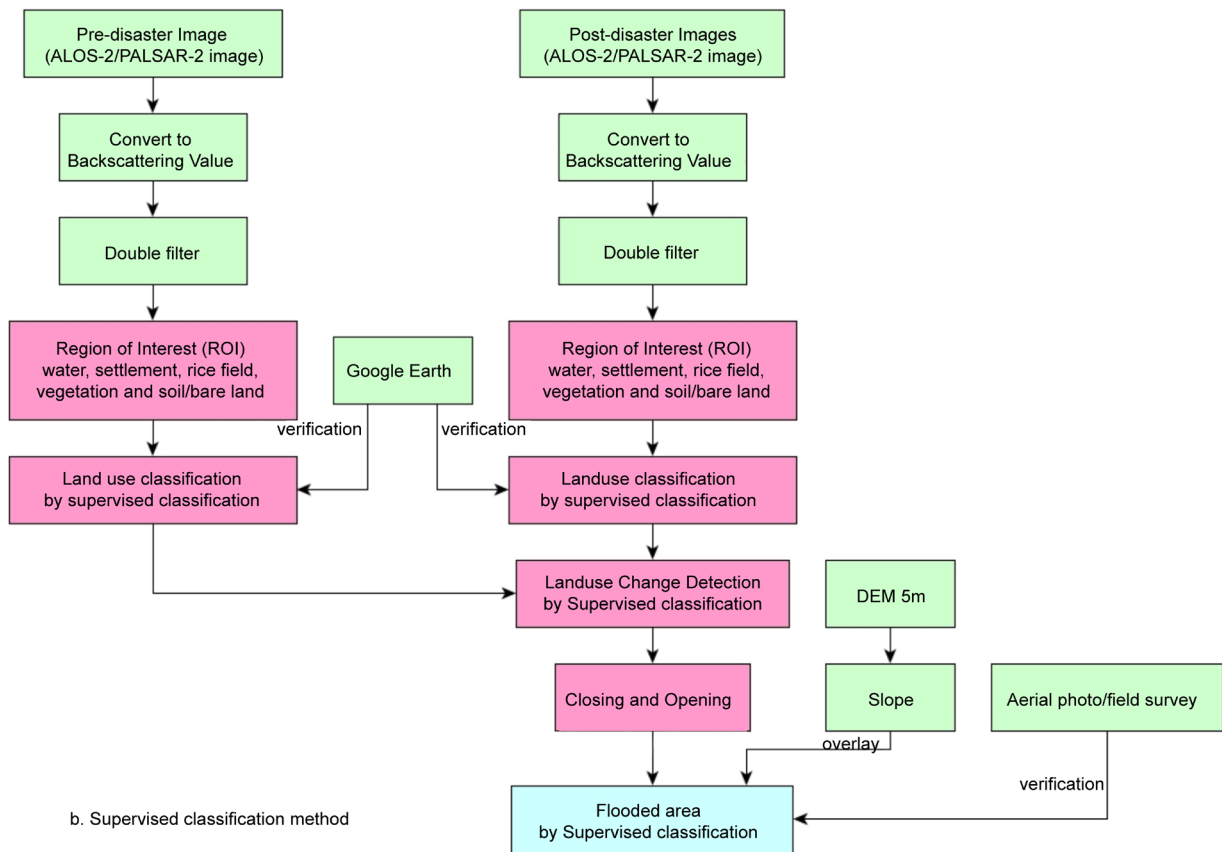
3.3. Double Filter

Speckle is noise on a radar image due to the phase fluctuations of the electromagnetic return signals [42] [43] [44]. It is difficult to interpret and images can be misclassified due to the speckle [45] [46] [47] [48]. Applying a filter is one method to reduce the speckle. There are two common types of filter; convolution



a. Unsupervised classification method

(a)



b. Supervised classification method

(b)

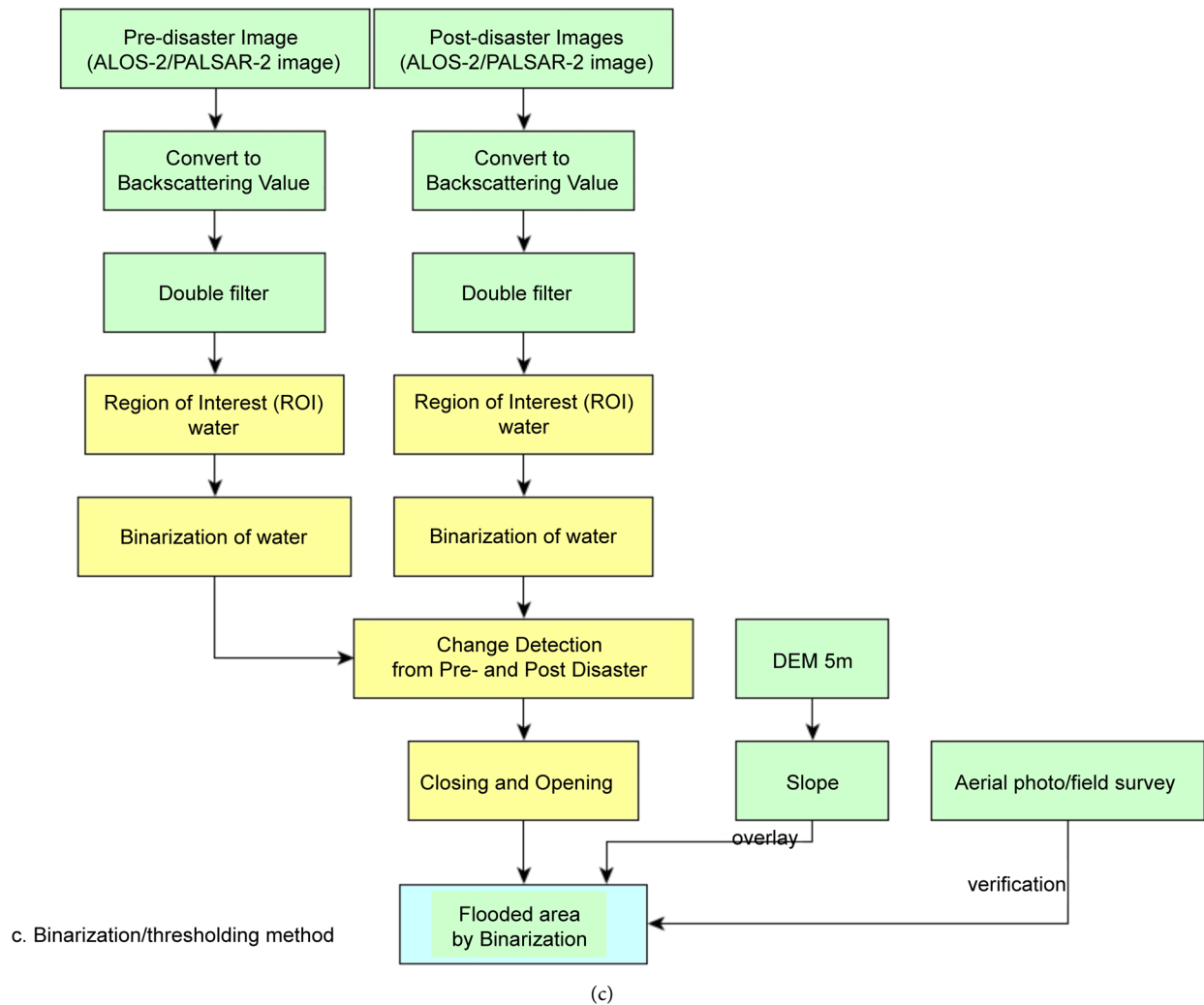


Figure 2. Flowchart of proposed methods; (a) unsupervised classification method, (b) supervised classification method and (c) binarization thresholding method.

Table 2. Value of CF and A for ALOS-2/PALSAR-2 [41].

CF	Mean (dB)	Std (dB)
CF ₁	-83.0	0.406
A	32.0	-

filter and adaptive filter [49]. Convolution filter reduced the speckle in the high strength signal area and had a smoothing effect [38] [50]. The adaptive filter reduced the speckle without eliminating the object detail [51]. When applying only one convolution filter or adaptive filter, it is called Single filter [38]. When utilizing the filter, the user has to decide the kernel size. Small kernel size was unable to remove the speckle, whereas big kernel size over-smoothed the image. The double filter was a solution to this problem [38].

The double filter is a new method to reduce the speckle by filtering an image two times using a different type of filter. This approach enhanced the ability to avoid misclassified pixels due to the speckle noise. The advantage of the double

filter was combining the superiority of two filters. This method produced images with less speckle noise, enhanced the edges and the object detail [38]. Rimba *et al.* recommends applying the Double filter for flood studies. By applying the Double filter, the classification of flooded and non-flooded area is more accurate compared to the Single filter. The recommended combination of filters was the combination of Local Sigma filter as the first filter and then Low Pass filter as the second filter. The ordering of filters has a different impact, e.g., the combination of filter 1 and filter 2 is different from the combination of filter 2 and filter 1.

3.4. Image Classification

3.4.1. Unsupervised Classification

Unsupervised classification: Pixels are classified based on the reflectance properties of pixels (*i.e.* clusters or group). The unsupervised classification method of image classification is used when no sample sites exist [52]. It is a grouping algorithm that customizes an iterative procedure to discrete image pixels into a spectrally similar group according to their position in spectral space [53]. There are several unsupervised classifying algorithms for images for example K-means and ISODATA. ISODATA was applied in this study by utilizing the software ENVI 5.3. The process of unsupervised classification starts by initiating the cluster of the pixel and calculating the mean of the cluster. During the iteration process, the similar characteristics of the pixel and closer distance is grouped into one class. The process is repeated until all the pixels are classified. By applying this method, we recognized the number of groups to create and which bands to apply and manually distinguish each group into new classifications. In Remote sensing application, unsupervised classification broadly used for land cover and land use classification [5] [54] [55], and coral habitat mapping [57]. The land cover was divided into 5 classes *i.e.* rice field, water, vegetation, building and soil or bare/open land area. We did the re-classify to the classified image from the software and then verified using Google Earth images.

3.4.2. Supervised Classification

Supervised classification: The user selects a representative training area for the digital image classification. Supervised classification in remote sensing field broadly utilized to classify the land cover and land use [4] [5] [6]. The image analysis software utilizes the training sites to classify the land cover categories in the whole image. The analysis of land cover is performed according to the spectral value determined in the training area. The frequently used supervised classification algorithms are maximum likelihood and minimum distance classification. Supervised classification steps are: select training areas, *i.e.* Region of Interest (ROI), generate the signature file and classify [52]. The clustering process of the supervised classification follows the same procedure as unsupervised classification. Supervised classification repeats the calculation of unclassified pixels to the same characteristics of the training area.

By following the training area of supervised classification, the software calculated pixels similar to the training area. In this study, the land use classified into

five classes; rice field, water, vegetation, building and soil or bare/open land area. The difference of unsupervised and supervised method is how to making the classification of land use. In unsupervised classification, we allowed the software ENVI 5.3 to classify the image. In supervised classification, we selected the ROI and asked the software to classify the pixels by their similarity or by distance.

3.4.3. Binarization

Image binarization is one of the fundamental techniques of image processing. Image binarization is a method that separates the pixel values into two groups, namely white as the background and black as foreground [54]. Thresholding has an important role in the binarization process, because the suitable threshold value is the beginning of the next process operation, e.g., feature extraction, segmentation, target recognition and so on [55].

The threshold method proposed by Otsu is a global adaptive binarization technique, which is the best representative of global adaptive thresholding and tries to find a single threshold value for the whole image [56]. Image thresholding is a simple arrangement of image segmentation. It is a way to create a binary image from a grayscale or full-color image [49].

Given an image $I(x, y)$ containing light object (change) on a dark background (no-change), the object may be extracted by a simple thresholding.

$$I(x, y) = \{1 \text{ } I(x, y) > T; 0 \text{ } I(x, y) < T\} \quad (3)$$

where; T is the threshold value given empirically or statistically by the researcher. All the pixels which are part of the object (change) are denoted 1, and the background (no change) are denoted 0 [3]. The local knowledge or visual interpretation about the scene or the area is meaningful in the thresholding method [57]. In this study, we only extracted the water for pre- and post-disaster images. When selecting the sample area of water by using ROI, we have to know the area very well. We can utilized the google earth data or other satellite images to verify the sample area, when we don't have local knowledge about the study area. After we found the difference of pre- and post-disaster image *i.e.* change detection, we decided the threshold of the flood area by utilizing the mean value of the change detection histogram.

3.5. Change Detection by Image Differencing

Change detection is a method of recognizing differences in the condition of an object or phenomenon by detecting it at different times. The conditions for using an image for change detection are fulfilled when having the images have the same area and are obtained at different times (t_1 and t_2) [58]. The formula of image differencing follows Equation (4).

$$I_d(x, y) = I_1(x, y) - I_2(x, y) \quad (4)$$

where I_1 and I_2 are the images generated from t_1 and t_2 , and (x, y) are positions of the pixels. The resulting image, I_d , denotes the intensity change of I_1 from I_2 . This technique works only if images are orthorectified/georeferenced.

The basic principle of change detection by applying remote sensing technology is that changes in land cover are seen according to the variation of radiance values; and the difference in radiance due to land cover change must be significant due to the other factors, e.g., atmospheric condition, difference sun angle and difference soil moisture [3].

In this study, the change detection approach was utilized to show the different of pre- and post-disaster images. It was applied after classification process of pre- and post-disaster images. The difference of classified object was identified as the flooded inundation area.

3.6. Opening and Closing

Opening and closing are two significant operators from mathematical morphology. Both of them derived from the fundamental operations of erosion and dilation. Opening and Closing were applied to binary images, although there are also gray level versions. The primary effect of an opening is somewhat like erosion in that it tends to remove some of the bright pixels (foreground) from the boundaries of regions of foreground pixels. However, it is less destructive than erosion in general. The impact of the operator is to preserve *foreground* regions for the opening process and background regions for the closing process that have a similar shape to this structuring element, or that can completely contain the structuring element while removing all other regions of foreground pixels for opening and background pixels for closing [59]. The purpose of this process was to generate a smooth classification result. This process required two classes of image. Thus, the classification image grouped into flooded area and non-flooded area.

3.7. Slope

The slope is the ratio of steepness or the degree of inclination of a feature relative to the horizontal plane. Gradient, grade, incline and pitch are used interchangeable with slope [60]. The slope is typically denoted as a percentage, an angle, or a ratio. The average slope of a topo feature can be measured from contour lines on a topo map or by DEM. The slope is achieved by dividing the rise over run. Multiply this ratio by 100 to calculate slope as a percentage. The slope angle represented in degrees is obtained by taking the arctangent of the ratio between rise and run [60]. **Table 3** lists the slope classification in percent and degree. The purpose of applying slope in this study was to remove the overestimate due to the shadow effect of SAR image. We did this step after generating flood predicting by three approaches.

4. Result and Discussion

The flood in Joso City occurred due to typhoon no.18 that caused torrential rains in the Kanto area and Tohoku area. The Kinugawa river discharge rate increased and caused the river bank to collapse. **Figure 3** shows the condition of the Kinugawa river; before the bank collapsed (recorded on May 6th, 2008 by GSI

Table 3. Slope classification [61].

Slope class	Slope (%)	Slope (degree)	Terminology
1	0 - 0.5	0	Level
2	>0.5 - 2	0.3 - 1.1	Near level
3	>2 - 5	>1.1 - 3	Very gentle slopes
4	>5 - 10	>3 - 5	Gentle slopes
5	>10 - 15	>5 - 8.5	Moderate slopes
6	>15 - 30	>8.5 - 16.5	Strong slopes
7	>30 - 45	>16.5 - 24	Very strong slopes
8	>45 - 70	>24 - 35	Extreme slopes
9	>70 - 100	>35 - 45	Steep slopes
10	>100	>45	Very steep slopes

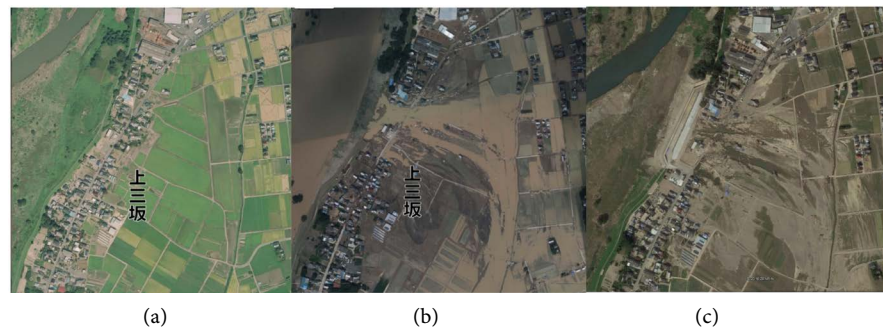


Figure 3. (a) Kinugawa River condition before collapse (May 6th, 2008) and (b) after collapse (September 11th, 2015). The image was orthorectified by Geospatial Information Authority of Japan (GSI). (c) Google Earth image (October 9th, 2015).

using the aerial photo) in **Figure 3(a)**, during the river bank collapse (recorded on September 11th, 2015 by GSI using the aerial photo) in **Figure 3(b)** and one month after the damage (recorded on October 9th, 2015 by Google Earth) in **Figure 3(c)**. The water of the Kinugawa River flowed to Joso City through this point. The river bank was repaired a few days after the flood.

The extraction methods were verified by using an aerial photo from GSI as shown in **Figure 4(a)**; it was recorded on September 11th, 2015 by aerial photography during the peak of the flood. The flood area is the blue line; it was manually delineated by using ArcGIS 10.2.2. Since it has high spatial resolution, the flooded area and non-flooded area can be distinguished clearly. **Figure 4(a)** was composed by Red Green Blue (RGB) from ALOS-2/PALSAR-2 image. The flood area was designated as the red color to show the contrast of flooded and non-flooded area. Thus, pre-disaster image filled red band; post-disaster image occupied green band, and the post-disaster image occupied Blue band. We selected the HH polarization for detecting the flood because water is easier to distinguish in this polarization [25]. Both of figures in **Figure 4** show a similar pattern of the flood. In order to extract the spatial information as shown in **Figure 4(b)** for further analysis (e.g., calculating the area, distribution, so on), the red

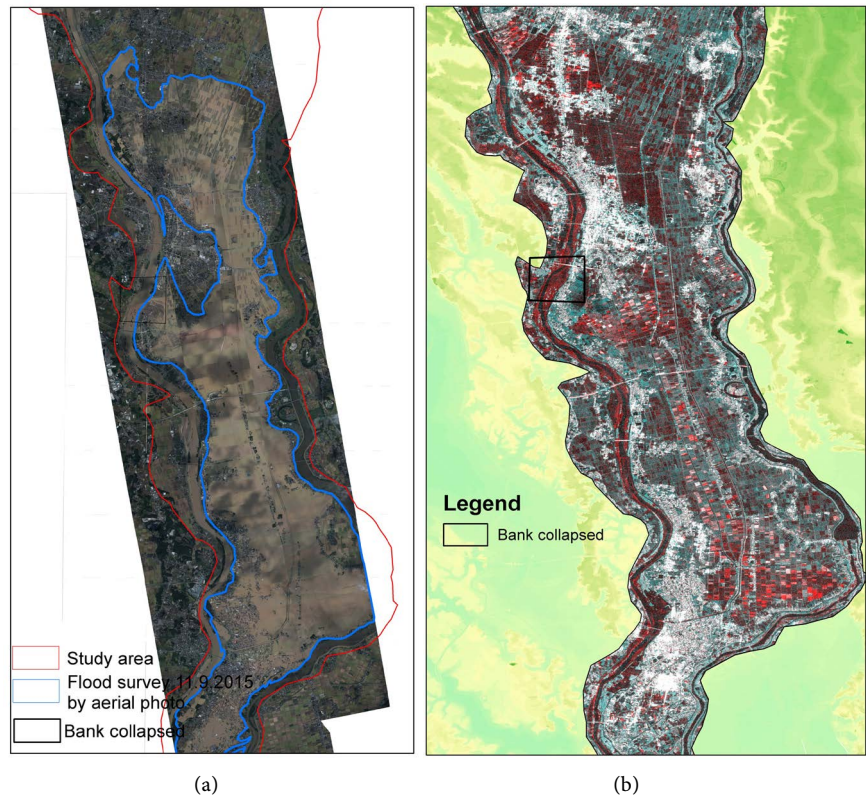


Figure 4. (a) Aerial photography by GSI; (b) Pre-and post-disaster RGB (before-after).

color in **Figure 4(b)** was extracted by 3 methods (unsupervised, supervised and binary/backscattering threshold).

4.1. Accuracy Assessment

Figure 5 shows the inundated flood extraction in Joso City by the three applied methods. It was recorded during the heavy raining. **Figure 5(a)** shows the unsupervised classification method to extract flood inundation, **Figure 5(b)** displays extraction of inundation area by the supervised classification method and **Figure 5(c)** extracted the flooded area by the binarization method. **Figure 5(a)** and **Figure 5(b)** were extracted by classifying the land use of pre- and post-disaster images. The land use was classified into five classes. The change detection of land use from the pre- and post-disaster was identified as flooded area.

As shown in **Figure 5(a)** and **Figure 5(b)**, unsupervised classification shows more overestimation than supervised classification. The reason unsupervised classification has overestimated results is because many classes of unsupervised classification have similar spectral [53]. We did not recommend this for classification activity if the user knows the study area well. This classification can be used when the user has no local knowledge of the area [62]. Supervised classification shows that flooded area is overestimated compared to the field survey (the black line shaded area is the field survey of flood inundation area). The pattern of the flood by supervised classification is un-cohesive as we can see in bottom

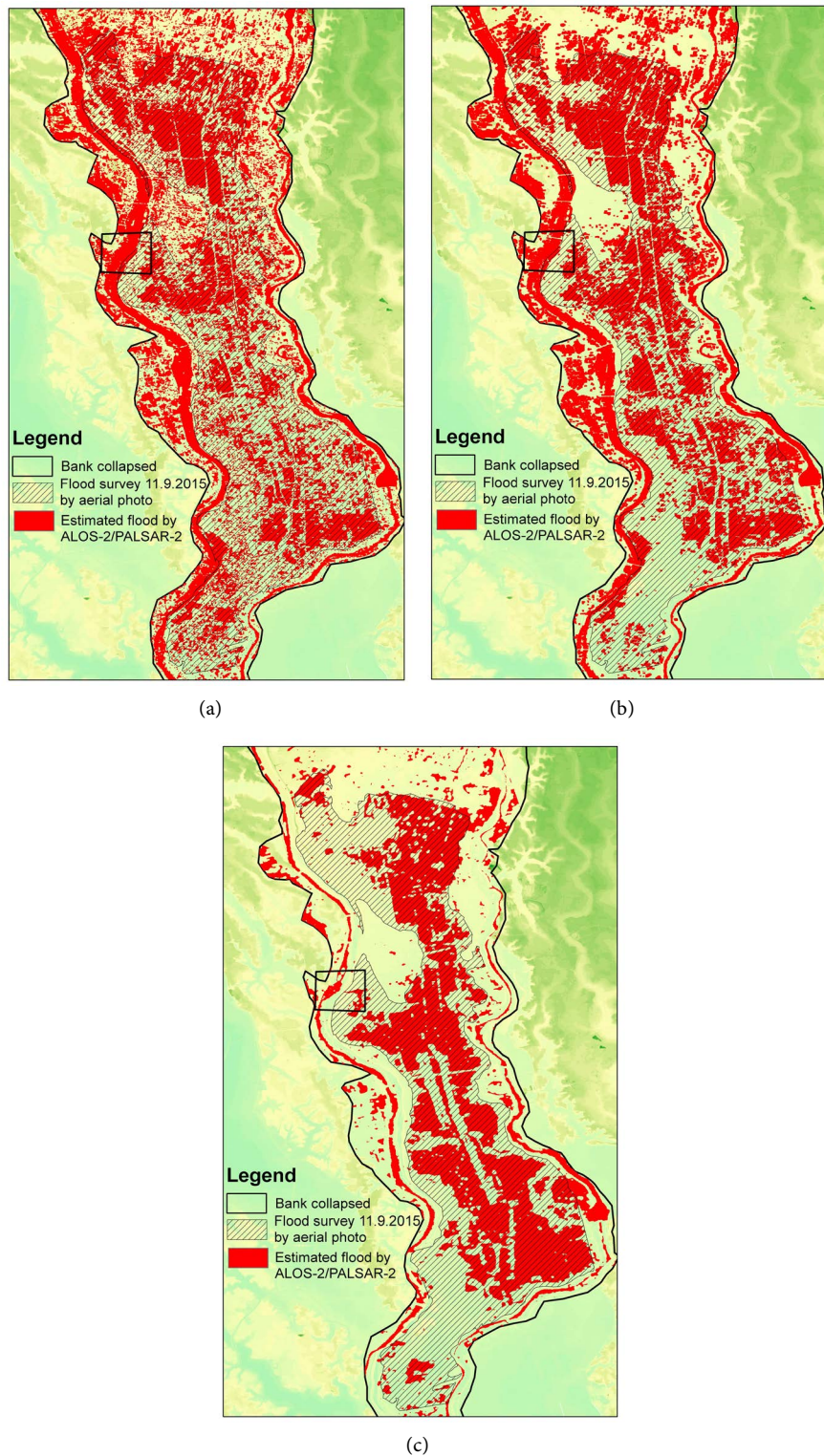


Figure 5. Estimation of flooded area by using methods; (a) Unsupervised classification, (b) Supervised classification and (c) Binary/Backscattering threshold.

part of flooded area. The supervised classification is unable to show the flooded area as one unit; the field survey, as illustrated in **Figure 4(a)**, shows that the flood distributes as one polygon. Comparing among the flood extraction me-

thods, binarization or thresholding the backscattering method displayed the flooding as one unit polygon. We found less overestimated area compared to the unsupervised and supervised method, especially in the top of the study area. When using unsupervised and supervised classification, the area that was wet due to the rain was identified as flooded area. Because the image was recording during rain, the soil moisture was very high. Thus, the wet soil has low backscattering as backscattering of water; the binarization could threshold the moisture level of the soil moister according to the mean value of the water histogram. Threshold process needs the local knowledge of the study area. Thus, we could generate the high accuracy of classification flooded and non-flooded area. Joso City was inundated due to the bank collapse, and the location of bank collapse can be seen in the black square in **Figure 5**. Applying unsupervised and supervised classification method did not show patterns of the bank collapse. The black box in **Figure 5(c)** shows a similar pattern to the field survey of bank collapse in **Figure 3**. Thus, binarization method was more informative than other methods.

We applied two kinds of accuracy assessment: overall accuracy and Kappa coefficient. Kappa coefficient has lower value than overall accuracy because kappa coefficient measures the agreement between the predicting map and reference data [63] [64]. It means that kappa accuracy measures the mistake and correct prediction. Overall accuracy is only measure the correct prediction (*i.e.* only measuring the diagonal of the matrix). Kappa efficient can be expressed by following Equation (5)

$$K = M \sum_{i=j=1}^r n_{ij} \sum_{i=j=1}^r n_i n_j / M^2 - \sum_{i=j=1}^r n_i n_j \quad (5)$$

where, r is the rows in the error matrix; n_{ij} is the number of observation in row, column j ; n_i is the total number of observation in row i ; n_j is the total number of observation in column j ; M is the number of observation in matrix. **Table 4** lists the result of accuracy assessment by statistic.

According to the statistic accuracy assessment in **Table 4**, Binary/backscattering threshold method shows the highest accuracy in overall accuracy and kappa coefficient comparing to other methods. We calculated this accuracy after removed the backscattering of building because it has effect double bouncing in SAR image. Hence, flooding in building area was difficult to detect. This study was considered a good accuracy due to the kappa coefficient 94%. A Kappa of 0.8 or above is considered as good accuracy; 0.4 or below is considered poor.

Table 4. Accuracy assessment of flood extraction approaches.

Extraction approaches	Accuracy assessment	
	Overall accuracy	Kappa coefficient
Unsupervised method	74%	69%
Supervised method	79%	72%
Binary/backscattering threshold	95%	94%

4.2. The Limitation of Using SAR Images

By using SAR images, overestimation due to the slant-range distortion, e.g., shadowing, could occur. Shadowing in slant range distortion occurs when the peak of the object, e.g., mountain covers the object's behind [65] [66]. We utilized the DEM data from GSI to generate the slope map. We checked the flooded area in Joso City by superimposing the extended flood with the slope map (Figure 6(a)) of Joso City. The flooded areas were less than 2%. Thus, we eliminated the flood estimation area which has slope more than 2%. The shadowed area which identified as the inundation area due to the slope were removed when its slope was more than 2%.

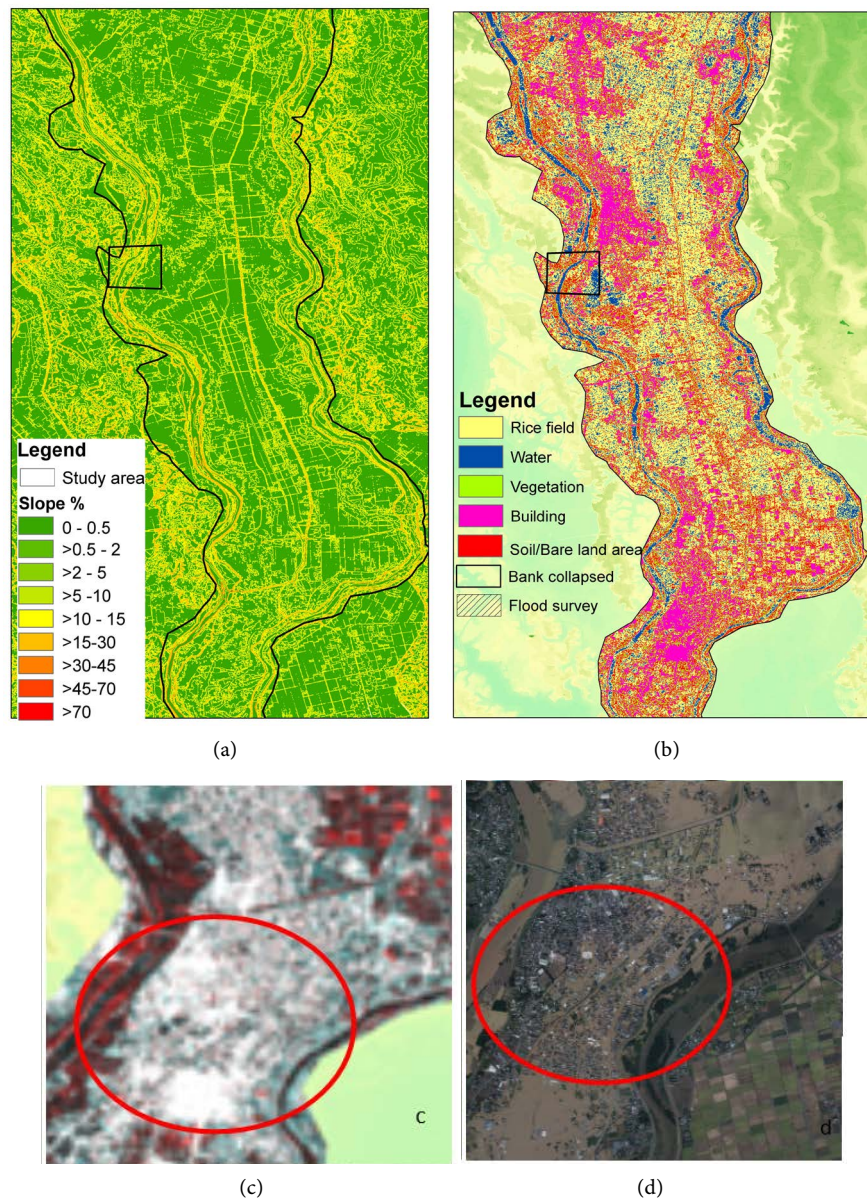


Figure 6. (a) Slope map, (b) Land use classification of pre-disaster image by supervised classification, (c) Building area in pre-and post-disaster RGB (before-after-after), (d) Building area in Aerial photography.

Figure 6(b) shows the land use distribution of Joso City before the flood. It shows that along the river was dominated by buildings or settlement and the center area of the study area was dominated by rice field. In **Figure 6(b)**, we emphasized the building area by red circle. **Figure 6(b)** shows high illuminating in ALOS-2/PALSAR-2 due to the double bounce effect in SAR images. Thus, the flood was unable to be detected. Nevertheless, this area was flooded as shown in **Figure 6(d)**. Another problem in utilizing SAR images was double bouncing of the signal to the sensor [67]. In this case, the signal from the sensor transmitted to the water and water reflected it back to the sensor. Unfortunately, the reflected signal from water was first reflected to the building before being reflected back to the sensor. Hence, the sensor received the signal of water backscattering as building backscattering. However, the sensor transmitted the signal to the building and the building reflected the signal back to the sensor. Thus, the sensor received signal from building twice, *i.e.*, double bouncing. This condition caused flood surrounding the building to be difficult to detect. It may be possible to detect this area by using different off nadir and polarization type. Different off nadir needs a difference of recording angle. Different polarization is different in transmitted and received signal.

5. Conclusions

We utilized ALOS-2/PALSAR-2 data in this study to find the fastest and most accurate method to extract the flood in Joso City. The flood was caused by typhoon No. 18 that brought heavy rainfall in the Tohoku region and Kanto region on September 2015. The binarization method was the most efficient in time and derived a more informative map from extracting the flood inundation compared to extracting the flood inundation using the land cover change by unsupervised and supervised classification. Using the binarization method, the flow pattern from the river collapse could be detected. The overall accuracy and kappa coefficient measured the accuracy assessment. Both of metric assessments show: Binary/backscattering threshold (94% for overall accuracy and 94% for kappa coefficient) was the highest accuracy compared to unsupervised classification (74% for overall accuracy and 69% for kappa coefficient) and supervised classification (79% for overall accuracy and 72% for kappa coefficient). Thus, binarization method is suitable for the rapid response of flooded area extraction.

Unsupervised and supervised classification showed overestimated flooded area. An unsupervised classification was more overestimated compared to the supervised classification because in the unsupervised classification categorized the pixel according to pixel distances or similarity of pixel characteristic. Hence, a number of similar classes were uncounted that led the misclassification. We do not recommend this classification system when the user knows the study area. An unsupervised classification was fully automatic because of the permission of the computer to classify the pixel. Supervised and the binarization method needs the local knowledge of the area. We could arrange the threshold of the water by using the binarization. Thus, this method was high accuracy compared to two

other methods. The binarization method can be applied to other areas and other SAR images for flood detection when the user has the local knowledge or the study area.

Overestimation of the flood inundation area due to shadowing effect in SAR image could be solved by using slope distribution. According to flood distribution found using field survey, the slope of the flooded area was less than 2%. This study utilized the HH polarization to detect the flood. Nevertheless, HH polarization cannot detect flooding in settlement areas. We utilized ALOS-2/PALSAR-2 image with 35.8° off-nadir angle. We will consider other polarization, e.g., VV, HV or VH and smaller or greater off-nadir angle to detect flooding in settlement areas for future work.

Acknowledgements

The authors are thanks to GSI for providing elevation data and field survey data, Joso City Government and Japan Aerospace Exploration Agency (JAXA) for ALOS-2/PALSAR-2 images. We also thank to Mr. Takumi Kajitani who explained the study area, Assoc. Prof. Takahiro Osawa, Mr. I Nyoman Sudi Parwata, Mr. Abd. Rahman As-syakur, Dr. Martiwi Diah Setiawati and Dr. Eng. Abu Bakar Sambah, for their great discussion during the study, and special thanks to Ms. Kira LaMarra Adams who proofread this manuscript.

References

- [1] Van Westen, C.J. (2000) Remote Sensing for Natural Disaster Management. *International Archives of Photogrammetry and Remote Sensing*, **33**, 1609-1617.
- [2] Guha-Sapir, D., Hoyois, P. and Below, R. (2015) Annual Disaster Statistical Review 2015; The Numbers and Trends. CRED and IRSS, Brussels, Centre for Research on the Epidemiology of Disasters (CRED) and Institute of Health and Society (IRSS).
- [3] Singh, A. (1989) Digital Change Detection Techniques Using Remotely-Sensed Data. *International Journal of Remote Sensing*, **10**, 989-1003.
<https://doi.org/10.1080/01431168908903939>
- [4] Rawat, J.S. and Kumar, M. (2015) Monitoring Land Use/Cover Change Using Remote Sensing and GIS Techniques: A Case Study of Hawalbagh Block, District Almorah, Uttarakhand, India. *The Egyptian Journal of Remote Sensing and Space Science*, **18**, 77-84. <https://doi.org/10.1016/j.ejrs.2015.02.002>
- [5] Hegazy, I.R. and Kaloop, M.R. (2015) Monitoring Urban Growth and Land Use Change Detection with GIS and Remote Sensing Techniques in Daqahlia Governorate Egypt. *International Journal of Sustainable Built Environment*, **4**, 117-124.
<https://doi.org/10.1016/j.ijsbe.2015.02.005>
- [6] Butt, A., Shabbir, R. and Sheikh, A.S. (2015) Land Use Change Mapping and Analysis Using Remote Sensing and GIS: A Case Study of Simly Watershed, Islamabad, Pakistan. *The Egyptian Journal of Remote Sensing and Space Science*, **18**, 251-259.
<https://doi.org/10.1016/j.ejrs.2015.07.003>
- [7] Alqurashi, A.F. and Kumar, L. (2013) Investigating the Use of Remote Sensing and GIS Techniques to Detect Land Use and Land Cover Change: A Review. *Advances in Remote Sensing*, **2**, 193-204.
- [8] Martino, L., Ulivieri, C., Jahjah, M. and Loret, E. (2009) Remote Sensing and GIS Techniques for Natural Disaster Monitoring. In: Olla, P., Ed., *Space Technologies*

for the Benefit of Human Society and Earth, Springer, 331-382.

- [9] Schumann, G.J.-P. (2015) Preface: Remote Sensing in Flood Monitoring and Management. *Remote Sensing*, **7**, 17013-17015.
<https://doi.org/10.3390/rs71215871>
- [10] Wiesmann, A., Wegmuller, M., Honikel, M., Strozzi, T. and Werner, C.L. (2001) Potential and Methodology of Satellite Based Sar for Hazard Mapping. *IEEE Proceeding of International Geoscience and Remote Sensing Symposium*, Vol. 7, Sydney, 9-13 July 2001, 3262-3264. <https://doi.org/10.1109/igarss.2001.978322>
- [11] Zhang, D.-W., *et al.* (2015) Flash Flood Hazard Mapping: A Pilot Case Study in Xiapu River Basin, China. *Water Science and Engineering*, **8**, 195-204.
<https://doi.org/10.1016/j.wse.2015.05.002>
- [12] Hapuarachchi, H.A.P., Wang, Q.J. and Pagano, T. (2011) A Review of Advances in Flash Flood Forecasting. *Hydrological Processes*, **25**, 2771-2784.
- [13] Davis, R.S. (2001) Flash Flood Forecast and Detection Methods. Severe Convective Storms. American Meteorological Society, Boston, 481-525.
- [14] Tamari, S. and Guerrero-Meza, V. (2016) Flash Flood Monitoring with an Inclined Lidar Installed at a River Bank: Proof of Concept. *Remote Sensing*, **8**, 834.
<https://doi.org/10.3390/rs8100834>
- [15] Yucel, I. (2015) Assessment of a Flash Flood Event Using Different Precipitation Datasets. *Natural Hazards*, **79**, 1889-1911.
<https://doi.org/10.1007/s11069-015-1938-9>
- [16] Singh, N., Vangani, N.S. and Sharma, J.R. (1993) Flash Flood Damage Mapping in Arid Environment Using Satellite Remote Sensing-A Case Study of Pali Region. *Journal of the Indian Society of Remote Sensing*, **21**, 75-86.
<https://doi.org/10.1007/BF02996345>
- [17] Kuldeep and Garg, P.K. (2016) The Role of Satellite Derived Data from Inundation Mapping Using GIS. *The International Archives of the Photogrammetry, Remote Sensing and Spatial Information Sciences*, **XL-3/W3**, 235-239.
- [18] Nascetti, A., *et al.* (2014) Fast Terrain Modelling for Hydrogeological Risk Mapping and Emergency Management: The Contribution of High-Resolution Satellite SAR Imagery. *Geomatics, Natural Hazards and Risk*, **6**, 554-582.
<https://doi.org/10.1080/19475705.2014.904824>
- [19] Campbell, J.B. and Wynne, R.H. (2011) Introduction to Remote Sensing Fifth Edition. The Guilford Press, New York.
- [20] Dellepiane, S., Bo, G., Monni, S. and Buck, C. (2000) SAR Images and Interferometric Coherence for Flood. *IEEE Proceeding of International Geoscience and Remote Sensing Symposium*, Vol. 6, Honolulu, 24-28 July 2000, 2608-2610.
- [21] Horritt, M.S., Mason, D.C. and Luckman, A.J. (2001) Flood Boundary Delineation from Synthetic Aperture Radar Imagery Using a Statistical Active Contour Model. *International Journal of Remote Sensing*, **22**, 2489-2507.
<https://doi.org/10.1080/01431160116902>
- [22] Wiesmann, A., Wegmuller, M., Honikel, M., Strozzi, T. and Werner, C.L. (2001) Potential and Methodology of Satellite Based SAR for Hazard Mapping. *IEEE Proceeding of International Geoscience and Remote sensing Symposium*, Vol. 7, Sydney, 9-13 July 2001, 3262-3264. <https://doi.org/10.1109/igarss.2001.978322>
- [23] Baldassarre, G.D., Schumann, G., Brandimarte, L. and Bates, P. (2011) Timely Low Resolution SAR Imagery to Support Floodplain Modelling: A Case Study Review. *Surveys in Geophysics*, **32**, 255-269.
<https://doi.org/10.1007/s10712-011-9111-9>

- [24] Richards, J.A. (2009) Scattering from Earth Surface Features. In: Remote Sensing with Imaging Radar. Springer, Berlin Heidelberg, 135-180.
- [25] Manjusree, P., Kumar, L.P., Bhatt, C.M., Rao, G.S. and Bhanumurthy, V. (2012) Optimization of Threshold Ranges for Rapid Flood Inundation Mapping by Evaluating Backscatter Profiles of High Incidence Angle SAR Images. *International Journal of Disaster Risk Science*, **3**, 113-122.
<https://doi.org/10.1007/s13753-012-0011-5>
- [26] Pierdicca, N., Marco, C. and Pulvirent, L. (2008) Integrating Physical and Topographic Information into a Fuzzy Scheme to Map Flooded Area by SAR. *Sensors*, **8**, 4151-4164.
- [27] Mason, D.C., *et al.* (2010) Flood Detection in Urban Areas Using TerraSAR-X. *IEEE Transactions on Geoscience and Remote Sensing*, **48**, 882-894.
<https://doi.org/10.1109/TGRS.2009.2029236>
- [28] Central Disaster Prevention Council (2016) Evacuation/Emergency Measures at Flood Damage. Central Disaster Prevention Council, Tokyo, Evacuation/Emergency Measures Examination Working Group at Flood Damage Working Group. (In Japanese)
- [29] Joso City Government (2016) Verification Report on the Response to the Kinugawa River Flood Damage in Joso City, 2015. Verification Report, Joso City Flood Damage Control Committee, Joso City. (In Japanese)
- [30] JAXA (2016) Japan Aerospace Exploration Agency (JAXA).
<http://global.jaxa.jp/projects/sat/alos2/>
- [31] Natsuaki, R., *et al.* (2016) Emergency Observation and Disaster Monitoring Performed by ALOS-2 PALSAR-2. *IEEE International Geoscience and Remote Sensing Symposium (IGARSS)*, Beijing, 10-15 July 2016, 3849-3852.
- [32] Rosenqvist, A., *et al.* (2014) Operational Performance of the ALOS Global Systematic Acquisition Strategy and Observation Plans for ALOS-2 PALSAR-2. *Remote Sensing of Environment*, **155**, 3-12. <https://doi.org/10.1016/j.rse.2014.04.011>
- [33] Honda, K., Fujihira, K., Asada, N., Fukushima, A. and Mushiake, N. (2016) Detecting Disaster Damage from 2015 Typhoon Etau by the Combined Use of Different SAR Satellites. *International Archives of the Photogrammetry, Remote Sensing and Spatial Information Sciences*, **XLI-B8**, 79-83.
- [34] Arii, M., Okada, Y. and Nishimura, T. (2016) Flooded Area Extraction from Time-Series ALOS-2 Data. *11th European Conference on Synthetic Aperture Radar (EUSAR2016)*, Hamburg, 6-9 June 2016.
- [35] Yamazaki, F. and Liu, W. (2016) Extraction of Flooded Area Due to the 2015 Kanto-Tohoku Heavy Rainfall in Japan Using PALSAR-2 Images. *The International Archives of the Photogrammetry, Remote Sensing and Spatial Information Sciences*, **XLI-B8**, 179-183.
- [36] Vassileva, M., Nascetti, A., Tonolo, F.G. and Boccoardo, P. (2015) Unsupervised Flood Extent Detection from SAR Imagery Applying Shadow Filtering from SAR Simulated Images. *IGARSS, Milan*, 2707-2710.
- [37] Hong, S., Jang, H., Kim, N. and Sohn, H.-G. (2015) Water Area Extraction Using RADARSAT SAR Imagery Combined with Landsat Imagery and Terrain Information. *Sensors*, **15**, 6652-6667. <https://doi.org/10.3390/s150306652>
- [38] Rimba, A.B., Miura, F., Setiwati, M.D., Sambah, A.B. and As-Syakur, A. (2016) The Effectivity of Double Filter to Reduce the Speckle and Detect Flood Inundation on ALOS/PALSAR. *37th Asian Conference on Remote Sensing*, Colombo, 17-21 October 2016.

- [39] Joso City (2016) Joso City.
http://www.city.joso.lg.jp/language/english/general_information/1446170618416.html
- [40] MLIT (2017) Introduction of the Kinugawa Flood. (In Japanese)
http://www.ktr.mlit.go.jp/shimodate/04_ryuik/ki01.htm
- [41] JAXA (2003) Japan Aerospace Exploration Agency.
<https://www.eorc.jaxa.jp/ALOS/en/about/palsar.htm>
- [42] Argenti, F., Lapini, A. and Bianchi, T. (2013) A Tutorial on Speckle Reduction in Synthetic Aperture Radar Images. *The IEEE Geoscience and Remote Sensing Magazine*, **1**, 6-35. <https://doi.org/10.1109/MGRS.2013.2277512>
- [43] Foucher, S. and Lopez-Martinez, C. (2014) Analysis, Evaluation, and Comparison of Polarimetric SAR Speckle Filtering Techniques. *IEEE Transactions on Image Processing*, **23**, 1751-1764. <https://doi.org/10.1109/TIP.2014.2307437>
- [44] Sumantyo, J.T.S. and Amini, J. (2008) A Model for Removal of Speckle Noise in SAR Images (ALOS PALSAR). *Canadian Journal of Remote Sensing*, **34**, 503-515.
- [45] Bazi, Y., Bruzzone, L. and Melgani, F. (2005) An Unsupervised Approach Based on the Generalized Gaussian Model to Automatic Change Detection in Multitemporal SAR Images. *IEEE Transactions on Geoscience and Remote Sensing*, **43**, 874-887. <https://doi.org/10.1109/TGRS.2004.842441>
- [46] Inglada, J. and Mercier, G. (2007) A New Statistical Similarity Measure for Change Detection in Multitemporal SAR Images and Its Extension to Multiscale Change Analysis. *IEEE Transactions on Geoscience and Remote Sensing*, **45**, 1432-1445. <https://doi.org/10.1109/TGRS.2007.893568>
- [47] Niu, X. and Ban, Y. (2013) Multi-Temporal RADARSAT-2 Polarimetric SAR Data for Urban Land-Cover Classification Using an Object-Based Support Vector Machine and a Rule-Based Approach. *International Journal Remote Sensing*, **34**, 1-26. <https://doi.org/10.1080/01431161.2012.700133>
- [48] Xi, R., Wang, Z., Xie, M. and Zhao, X. (2015) A Non-Local Vectorial Total Variational Model for Multichannel SAR Image Speckle Suppression. *Chinese Journal of Aeronautics*, **28**, 770-779. <https://doi.org/10.1016/j.cja.2015.03.012>
- [49] ENVI (2004) ENVI User's Guide.
http://aviris.glfcen.uba.ar/Curso_SR/biblio_sr/ENVI_userguide.pdf
- [50] North, H.C. and Wu, Q.X. (2001) An Edge Preserving Filter for Imagery Corrupted with Multiplicative Noise. *Photogrammetric Engineering & Remote Sensing*, **67**, 57-64.
- [51] Jensen, J.R. (2004) Introductory Digital Image Processing—A Remote Sensing Perspective. 3rd Edition, Prentice Hall, New Jersey.
- [52] GIS Geography (2016) GIS Geography.
<http://gisgeography.com/image-classification-techniques-remote-sensing/>
- [53] Enderle, D.I.M. and Weih Jr, R.C. (2005) Integrating Supervised and Unsupervised Classification Methods to Develop a More Accurate Land Cover Classification. *Journal of the Arkansas Academy of Science*, **59**, 65-73.
- [54] Han, S.Q. and Wang, L. (2002) A Survey of Thresholding Methods for Image Segmentation. *Systems Engineering and Electronics*, **24**, 91-95.
- [55] Zhang, W. and Dou, J. (2014) A Fast Thresholding Technique in Image Binarization for Embedded System. *TELKOMNIKA Indonesian Journal of Electrical Engineering*, **12**, 592-598.
- [56] Otsu, N. (1979) A Threshold Selection Method from Grey-Level Histogram. *IEEE Transactions on Systems, Man, and Cybernetics*, **9**, 62-66.

<https://doi.org/10.1109/TSMC.1979.4310076>

- [57] Schowengerdt, R.A. (1983) Techniques for Image Processing in Remote Sensing. Academic Press, New York.
- [58] İlsever, M. and Unsalan, C. (2012) Pixel-Based Change Detection Methods. Online Version: Springer Brifs in Computer Science.
- [59] HIPR2 (2004) Image Processing Learning Resources.
http://homepages.inf.ed.ac.uk/rbf/HIPR2/hipr_top.htm
- [60] Geokov (2012) Geokov Education.
<http://geokov.com/education/slope-gradient-topographic.aspx>
- [61] Haynes, R.H. (1998) The Canadian System of Soil Classification. 3rd Edition, NRC Research Press, Ottawa.
- [62] Tempfli, K., Kerle, N., Huurneman, G.C. and Janssen, L.L.F. (2009) Principle of Remote Sensing. The International Institute for Geo-Information Science and Earth Observation (ITC), Enschede.
- [63] Lillisand, T.M, Keifer, R.W. and Chipman (2004) Remote Sensing and Image Interpretation. John Wiley and Sons, New York.
- [64] Danoedoro, P. (2012) Pengantar Penginderaan Jauh Digital. Penerbit Andi Yogyakarta, Yogyakarta. (In Indonesia)
- [65] SARMap (2009) SARMap 2008. Synthetic Aperture Radar and SARscape. Purasca, Croglio.
- [66] Samuel, W., McCandless, J. and Jackson, C.R. (2004) Chapter 1. Principle of Synthetic Aperture Radar. In: *SAR Marine User's Manual*, NOAA/NESDIS, Washington DC, 1-23.
- [67] Hong, S.-H. and Wdowinski, S. (2013) Double-Bounce Component in Cross-Polarimetric SAR from a New Scattering Target Decomposition. *IEEE Transactions on Geoscience and Remote Sensing*, **52**, 3039-3051.



Submit or recommend next manuscript to SCIRP and we will provide best service for you:

Accepting pre-submission inquiries through Email, Facebook, LinkedIn, Twitter, etc.

A wide selection of journals (inclusive of 9 subjects, more than 200 journals)

Providing 24-hour high-quality service

User-friendly online submission system

Fair and swift peer-review system

Efficient typesetting and proofreading procedure

Display of the result of downloads and visits, as well as the number of cited articles

Maximum dissemination of your research work

Submit your manuscript at: <http://papersubmission.scirp.org/>

Or contact gep@scirp.org